

Dynamical structure factor and a new method to measure the pairing gap in two-dimensional attractive Fermi-Hubbard model

Huaisong Zhao,* Peng Zou,† and Feng Yuan

College of Physics, Qingdao University, Qingdao 266071, China

By calculating the dynamical structure factor along the high symmetry directions in the Brillouin zone, the dynamical excitations of attractive Fermi-Hubbard model in a two-dimensional square optical lattice are studied with random phase approximation. Two kinds of collective modes are investigated, including a Goldstone phonon mode at transferred momentum $\mathbf{q} = [0, 0]$ and a roton mode at $\mathbf{q} = [\pi, \pi]$. The phonon originates from the spontaneously U(1) symmetry breaking of pairing gap, and its speed is suppressed by the interaction strength. The collective roton mode originates from the breaking of a global pseudospin SU(2) symmetry. Dynamical excitations at $\mathbf{q} = [\pi, \pi]$ consist of a sharp roton molecular peak in the low-energy region and a broad atomic excitation band in the higher energy region. Furthermore, the weight of the roton molecular peak decreases monotonically with increasing the hopping strength, while the weight of the atomic excitations increases quickly. Interestingly we check that the area covered by the roton molecular peak scales with the square of the pairing gap, which is also true in the system with spin-orbit coupling. This conclusion paves a potential way to measure the pairing gap of lattice system experimentally by measuring the dynamical structure factor at $\mathbf{q} = [\pi, \pi]$.

I. INTRODUCTION

The superfluid state of a quantum many-body Fermi atomic gases has a non-zero pairing gap (or order parameter) due to the Cooper pairing physics. Finding a convenient way to measure the pairing gap is essential to understand many-body pairing phenomenon and dynamical excitations. Currently the pairing gap are mainly gained by all kinds of excited progresses, like momentum-resolved photo-emission spectroscopy [1, 2], or radio-frequency spectroscopy [3–5]. However, it is difficult to measure the pairing gap when the band structure becomes complex owing to the appearance of magnetic fields or spin-orbit coupling (SOC) [6–11]. Moreover, dynamical excitations are also an important method to study pairing correlation information. Dynamical excitations can be investigated from the dynamical structure factor, which is the Fourier transformation of the density-density correlation function in the momentum and energy representation and reflects the two-body correlation physics directly. Experimentally the dynamical structure factor can be directly measured by a two-photon Bragg scattering technique [12–18].

In continuous Fermi gases, usually the collective modes are studied at a small transferred momentum q , while the single-particle excitations of the unpaired and paired atoms are usually shown at a relatively larger q . Specifically the excitations of the paired atoms correspond to the bosonic molecular excitations. In 2008, C. J. Vale experimental group studied the single-particle excitations at a large transfer momentum $q \gg k_F$, and found that the molecular scattering peak takes up a more and more significant weight when tuning the interaction from the

Bardeen-Cooper-Schrieffer (BCS) part to Bose-Einstein-Condensate (BEC) regime, different from the behaviour of atomic scattering [12]. Later they investigated the Goldstone phonon mode and pair-breaking excitation at a small transferred momentum [13], and found that the sound speed is suppressed by the strong interaction. In 2022, H. Biss *et al* experimentally studied the phonon dispersion through the whole BCS-BEC crossover by using the same Bragg spectrum [14]. Theoretically the dynamical structure factors of three-dimensional (3D) Fermi gases had been studied quite a lot [19–27]. For two-dimensional (2D) superfluid Fermi gases, recently the dynamical structure factor at different values of interaction strength was measured by the two-photon Bragg scattering technique [28]. The exact quantum Monte Carlo (QMC) method had been used to calculate the dynamical structure factor at a large transferred momentum, by which E. Vitali *et al.* investigated the weight change of both the molecular excitations and atomic excitations [29]. For other low-dimensional Fermi gases, several theoretical works had been carried out to study the dynamical excitation with dynamical structure factor [30, 31].

As to the discrete ultracold atomic gases, an optical lattice generated by superimposing orthogonal standing waves can be widely used to simulate the physics in crystal environment [32, 33], and the system can be described by the Bose-Hubbard model or Fermi-Hubbard model [34–46]. Several theoretical groups have studied the attractive Fermi-Hubbard model, which is closely related to the strongly correlated systems in condensed matter physics [47–57]. Experimentally the attractive Fermi-Hubbard model in cold atoms had been realized [58–63]. To date, there is no two-photon Bragg spectroscopy experiment on 2D Fermi gases in an optical lattice. In 2020, E. Vitali *et al* numerically simulated the dynamical structure factor along the high symmetry directions of the Brillouin zone (BZ) with the attractive Fermi-Hubbard model in a square optical lattice at half-filling [64], and

* hszhao@qdu.edu.cn

† phy.zoupeng@gmail.com

gave the low-energy Nambu-Goldstone collective mode and single-particle excitations in the higher energy region. However, there is no work to study the molecular excitations in this discrete system, which is closely related to the pairing gap. In this paper, we theoretically investigate dynamical excitations of 2D Fermi superfluid in an optical lattice from the weak coupling regime to the intermediate coupling regime, and analyze the main characteristics of dynamical behaviour in both collective and single-particle excitations.

In general, the doping to the system can change the Fermi energy, and then go on influencing related dynamical excitations. Therefore it is interesting to investigate the dynamical excitations at different doping. In this paper, we focus on the change of dynamical excitations from the half-filling to the doped cases. In particular, we will show that the roton molecular peak at the momentum $\mathbf{q} = [\pi, \pi]$ provides a simple strategy to measure the pairing gap in doped system, since the square of the pairing gap is proportional to the area covered by this roton molecular peak. Moreover, this strategy to measure pairing gap can be generalized to other Fermi atomic gases with SOC in an optical lattice, where it is hard to measure pairing gap directly owing to the complex band structure [65].

This paper is organized as follows. In the next section, we will use the motion equation of Green's function to solve the 2D Fermi-Hubbard model in mean field approximation, and self-consistently obtain the chemical potential and pairing gap. In Sec. III, we introduce how to calculate dynamical structure factor with random phase approximation (RPA). We display results of dynamic structure factor at half-filling and compare with the QMC results in Sec. IV. In Sec. V, we introduce results when the system is away from half-filling, and discuss the hopping dependence of the sound speed and the dynamical excitations at a transferred momentum $\mathbf{q} = [\pi, \pi]$, and check the doping dependence of dynamical structure factor in Sec. VI. Finally we give our conclusions and acknowledgment, and provide some calculation details in the appendix.

II. MODEL AND HAMILTONIAN

An attractive Fermi-Hubbard model in 2D square optical lattices can be described by a Hamiltonian in spatial representation as follows:

$$H = -t \sum_{\langle ij \rangle} C_{i\sigma}^\dagger C_{j\sigma} - \mu \sum_i C_{i\sigma}^\dagger C_{i\sigma} - U \sum_i C_{i\uparrow}^\dagger C_{i\downarrow}^\dagger C_{i\downarrow} C_{i\uparrow}, \quad (1)$$

where $\langle ij \rangle$ means the nearest-neighbor sites of lattice. $C_{i\sigma}^\dagger$ ($C_{i\sigma}$) is the creation (annihilation) operator of a particle with spin σ , hopping energy t and chemical potential μ at site i . The Hubbard energy $U > 0$ is just

the strength of on-site two-body attraction interaction. In the following discussions, U is set to be the unit energy, while the lattice length a_0 is used as unit length. Within the mean field theory, the four-operators interaction Hamiltonian can be dealt into a two-operators one with the definition of pairing gap $\Delta = U \langle C_{i\downarrow} C_{i\uparrow} \rangle$. The pairing gap Δ can be chosen to be a real number in the ground state. Then the above Hamiltonian is displayed into a mean field one, whose expression in momentum space reads

$$H_{\text{MF}} = \sum_{\mathbf{k}, \sigma} \xi_{\mathbf{k}} C_{\mathbf{k}\sigma}^\dagger C_{\mathbf{k}\sigma} - \sum_{\mathbf{k}} (\Delta^* C_{\mathbf{k}\downarrow} C_{-\mathbf{k}\uparrow} + H.c.) + \frac{|\Delta|^2}{U}, \quad (2)$$

where $\xi_{\mathbf{k}} = -Zt\gamma_{\mathbf{k}} - \mu$ and $\gamma_{\mathbf{k}} = (\cos k_x + \cos k_y)/2$. The nearest lattice number satisfies $Z = 4$ for 2D square lattice.

The above mean field Hamiltonian can be solved by motion equations of Green's function. Here we define the diagonal Green's function $G(\mathbf{k}, \tau - \tau') = -\langle T_\tau C_{\mathbf{k}\sigma}(\tau) C_{\mathbf{k}\sigma}^\dagger(\tau') \rangle$ and off-diagonal one $\Gamma^\dagger(\mathbf{k}, \tau - \tau') = -\langle T_\tau C_{-\mathbf{k}\uparrow}^\dagger(\tau) C_{\mathbf{k}\downarrow}^\dagger(\tau') \rangle$, respectively. The diagonal Green's function is related to the normal particle density and the off-diagonal Green's function is related to the singlet Cooper pairing information. Their expressions in momentum and energy representation are given by

$$G(\mathbf{k}, \omega) = \frac{1}{2} \left(\frac{1 + \xi_{\mathbf{k}}/E_{\mathbf{k}}}{\omega - E_{\mathbf{k}}} + \frac{1 - \xi_{\mathbf{k}}/E_{\mathbf{k}}}{\omega + E_{\mathbf{k}}} \right) \quad (3a)$$

$$\Gamma^\dagger(\mathbf{k}, \omega) = \frac{\Delta^*}{2E_{\mathbf{k}}} \left(\frac{1}{\omega - E_{\mathbf{k}}} - \frac{1}{\omega + E_{\mathbf{k}}} \right), \quad (3b)$$

where $E_{\mathbf{k}} = \sqrt{\xi_{\mathbf{k}}^2 + |\Delta|^2}$ is the quasiparticle spectrum. The chemical potential μ and pairing gap Δ are determined by self-consistently solving the density equation and pairing gap equation

$$n = \frac{1}{2} \sum_{\mathbf{k}} \left(1 - \frac{\xi_{\mathbf{k}}}{E_{\mathbf{k}}} \right) \tanh \left(\frac{E_{\mathbf{k}}}{2T} \right),$$

$$1 = \frac{U}{N} \sum_{\mathbf{k}} \frac{1}{2E_{\mathbf{k}}} \tanh \left(\frac{E_{\mathbf{k}}}{2T} \right), \quad (4)$$

We have set Boltzmann constant $k_B = 1$, and will consider a typical low temperature $T/U = 0.01$ (close to zero) in the following.

Generally increasing hopping energy t will decrease the value of pairing gap Δ . The relation between Δ and t at different density n is shown in Fig. 1. The pairing gap will close to zero at a large enough hopping energy t , which marks the edge of a phase transition between superfluid state to a normal state. Moreover, Δ is clearly suppressed as particle density n decreases. It should be noted that the mean field pairing gap is larger than the results of the QMC [64]. For example, for $t/U = 0.25$

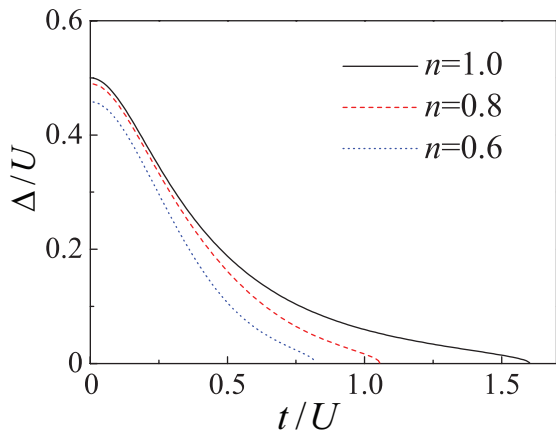


Figure 1. Pairing gap Δ as a function of t for $n = 1.0$ (black solid line), $n = 0.8$ (red dashed line) and $n = 0.6$ (blue dotted line).

at half-filling ($n = 1.0$), the mean field theory gives $\Delta/U = 0.345$, while QMC predicts $\Delta/U = 0.1825$. Experimentally the formation and spatial ordering of nonlocal fermion pairs in an attractive Fermi-Hubbard system are observed by using a two-species gas of degenerate ^{40}K atoms [63].

III. DYNAMICAL STRUCTURE FACTOR AND RANDOM PHASE APPROXIMATION

In this section, we will introduce the main idea of RPA, which is a beyond mean field strategy of treating fluctuation part in Hamiltonian to investigate dynamical excitations.

In superfluid state, there are four different densities. Besides the normal spin-up $\hat{n}_1 = \langle C_{i\uparrow}^\dagger C_{i\uparrow} \rangle$ and spin-down density $\hat{n}_2 = \langle C_{i\downarrow}^\dagger C_{i\downarrow} \rangle$, the anomalous density $\hat{n}_3 = \langle C_{i\downarrow} C_{i\uparrow} \rangle$ and its complex conjugate $\hat{n}_4 = \langle C_{i\uparrow}^\dagger C_{i\downarrow}^\dagger \rangle$ are important to describe Cooper pairing. These four densities are coupled with each other due to a non-zero interaction, and any perturbation in one density will induce density fluctuation in other densities. In the frame of linear response theory, the small external perturbation potential V_{ext} and density fluctuations δn are connected with each other by response function of the system χ , namely $\delta n = \chi V_{\text{ext}}$.

Actually the mean-field theory neglects the contribution from the fluctuation term of interaction Hamiltonian, and so can not give a good prediction about the dynamical excitations of an interacting system. In order to take fluctuation part back [66–68], the random phase approximation (RPA) has been verified to be a good method to calculate response function χ beyond the mean-field theory. In 3D BCS-BEC crossover Fermi superfluid, predictions about dynamical excitations from

this method even quantitatively agree well with that in experiments [14, 21, 23]. The 2D theoretical results of this method qualitatively agree with the QMC data [30]. So it is reasonable to expect that this RPA strategy can provide a qualitatively reliable prediction for 2D lattice Fermi superfluid.

The main idea of RPA is to treat fluctuation Hamiltonian as part of an effective external potential, by which find that the response function χ beyond mean field theory is connected to its mean-field approximation χ^0 by

$$\chi(\mathbf{q}, i\omega_n) = \frac{\chi^0(\mathbf{q}, i\omega_n)}{\hat{1} + \chi^0(\mathbf{q}, i\omega_n)UG}. \quad (5)$$

Here $G = \sigma_0 \otimes \sigma_x$ is a direct product of unit matrix σ_0 and Pauli matrix σ_x .

The numerical calculation of mean-field response function χ^0 is very easy, and its expression is given by the following matrix

$$\chi^0(\mathbf{q}, i\omega_n) = \begin{bmatrix} \chi_{11}^0 & \chi_{12}^0 & \chi_{13}^0 & \chi_{14}^0 \\ \chi_{21}^0 & \chi_{22}^0 & \chi_{23}^0 & \chi_{24}^0 \\ \chi_{31}^0 & \chi_{32}^0 & \chi_{33}^0 & \chi_{34}^0 \\ \chi_{41}^0 & \chi_{42}^0 & \chi_{43}^0 & \chi_{44}^0 \end{bmatrix}. \quad (6)$$

The dimension of χ^0 reflect the coupling situation among four different densities. These 16 matrix elements are determined by the corresponding density-density correlation functions which can be obtained by a set of Green's functions defined before. Due to all possible symmetries of system, only 6 of these matrix elements are independent, i.e., $\chi_{11}^0 = \chi_{22}^0$, $\chi_{12}^0 = \chi_{21}^0 = -\chi_{33}^0 = -\chi_{44}^0$, $\chi_{31}^0 = \chi_{32}^0 = \chi_{14}^0 = \chi_{24}^0$, $\chi_{41}^0 = \chi_{42}^0 = \chi_{13}^0 = \chi_{23}^0$. The symmetry of the matrix is closely related to the symmetry of the Green's functions, such as $\Gamma^\dagger(\mathbf{k}, \omega) = \Gamma(\mathbf{k}, \omega) = \Gamma(\mathbf{k}, -\omega)$, which leads to $\chi_{12}^0 = \chi_{21}^0$, where $\chi_{12}^0 = -\langle T_\tau C_{i\uparrow}^\dagger(\mathbf{r}, \tau) C_{i\uparrow}(\mathbf{r}, \tau) C_{i\downarrow}^\dagger(\mathbf{r}', \tau') C_{i\downarrow}(\mathbf{r}', \tau') \rangle$. Based on Wick's theorem, $\chi_{12}^0 = -\Gamma^\dagger(\mathbf{r} - \mathbf{r}', \tau - \tau') \Gamma(\mathbf{r}' - \mathbf{r}, \tau' - \tau)$. Their expressions are listed in the final appendix of this paper.

The total density response function χ_n is defined by $\chi_n \equiv \chi_{11} + \chi_{12} + \chi_{21} + \chi_{22}$, its expression after RPA treatment is given by

$$\chi_n(\mathbf{q}, i\omega_n) = \frac{2\chi_1}{\chi_2 + U\chi_1}, \quad (7)$$

where

$$\chi_1 = \begin{vmatrix} \chi_{11}^0 + \chi_{12}^0 & 2\chi_{14}^0 U & 2\chi_{13}^0 U \\ \chi_{14}^0 & 1 + \chi_{34}^0 U & -\chi_{12}^0 U \\ \chi_{13}^0 & -\chi_{12}^0 U & 1 + \chi_{43}^0 U \end{vmatrix} \quad (8a)$$

$$\chi_2 = \begin{vmatrix} 1 + \chi_{34}^0 U & -\chi_{12}^0 U \\ -\chi_{12}^0 U & 1 + \chi_{43}^0 U \end{vmatrix}. \quad (8b)$$

According to the fluctuation-dissipation theory, the density dynamical structure factor $S(\mathbf{q}, \omega)$ is connected to the imaginary part of the density response function χ_n by

$$S(\mathbf{q}, \omega) = -\frac{1}{\pi} \text{Im} \chi_n(\mathbf{q}, i\omega_n \rightarrow \omega + i\delta), \quad (9)$$

where \mathbf{q} and ω are respectively the transferred momentum and energy. δ is a small positive number in numerical calculation (usually we set $\delta = 0.003$).

IV. RESULTS AT HALF-FILLING

We firstly discuss the dynamical structure factor of 2D attractive Fermi-Hubbard model at half-filling, namely $n = 1$. By analyzing the density dynamical structure factor under different transfer momenta, one can obtain collective excitations and single-particle excitations of Fermi atomic gases. We have calculated the energy and momentum dependence of density dynamical structure factor $S(\mathbf{q}, \omega)$, and obtain the contour plot of $S(\mathbf{q}, \omega)$ along the high symmetry directions in the BZ for different hopping strength. The results are shown in Fig. 2. In the low-energy region, $S(\mathbf{q}, \omega)$ displays sharp peaks, which denotes two gapless collective modes. The first one starts from $\mathbf{q} = [0, 0]$ and increases almost linearly in the low-momentum region along with $[0, 0] \rightarrow [\pi, 0]$ or $[0, 0] \rightarrow [\pi, \pi]$. This collective mode is the phonon mode which origins from the spontaneously U(1) symmetry breaking of pairing gap (or order parameter). The slope of this mode at $\mathbf{q} = [0, 0]$ gives the speed of phonon. The other collective one is roton mode appearing around $\mathbf{q} = [\pi, \pi]$. The roton mode can be understood by the breaking of a global pseudospin SU(2) symmetry [68, 71, 72]. There is a degeneracy between superfluid and charge density wave (CDW). In this paper, we don't discuss the competition between them. As the momentum increases, the phonon mode gradually merges into the single-particle excitations, and shows a finite expansion width because of the scattering with the single-particle excitations. The appearance of two collective modes had been confirmed by the QMC simulations [64].

In the high-energy region, the excitations come into a single-particle region dominated by the pair-breaking effect. The two atoms in a Cooper pair both come from quasiparticle spectrum $E_{\mathbf{k}}$, and require energy $E_{\mathbf{k}+\mathbf{q}} + E_{\mathbf{k}}$ to break Cooper pairs at a certain transferred momentum q . This pair-breaking physics forms a continuous excitation regime, and the minimum energy $\min[E_{\mathbf{k}+\mathbf{q}} + E_{\mathbf{k}}]$ is labeled by a yellow dotted line in Fig. 2b. This yellow horizontal line is located at the transferred energy $\omega = 2\Delta$, denoting one way to measure pairing gap. However, this strategy to measure the pairing gap suffers from difficulty for other system with complex band structure brought by complex interaction like SOC. And the minimum energy will not be a horizontal line. A larger t will make the horizontal threshold move to the low-binding energy region since the pairing gap decreases. Moreover, the upper branch of the single-particle excitations based on QMC appears at a significantly lower energy with respect to the RPA result. This may be related to the many-body interaction beyond the RPA theory. By introducing the quasiparticle coherent weight Z_F [74–77], we try to understand the QMC results.

For simplicity, we introduce a full Green's function including the self-energy of many-body interaction in the normal state, namely, $g(\mathbf{k}, \omega) = 1/(\omega - \xi_{\mathbf{k}} - \Sigma(\mathbf{k}, \omega))$, where $\Sigma(\mathbf{k}, \omega)$ is the self-energy and can be decoupled as $\Sigma(\mathbf{k}, \omega) = \Sigma_e(\mathbf{k}, \omega) + \omega\Sigma_o(\mathbf{k}, \omega)$. We define the quasiparticle coherent weight as: $Z_F^{-1}(\mathbf{k}, \omega) = 1 - \Sigma_o(\mathbf{k}, \omega)$. Under the static limit approximation, $Z_F = Z_F(\mathbf{k} = \mathbf{k}_F, \omega = 0)$ by taking the Fermi momentum $\mathbf{k} = \mathbf{k}_F$. The full Green's function has a simple form $g(\mathbf{k}, \omega) = Z_F/(\omega - Z_F\xi_{\mathbf{k}}) = Z_F/(\omega - \tilde{\xi}_{\mathbf{k}})$, where $\tilde{\xi}_{\mathbf{k}} = Z_F\xi_{\mathbf{k}}$ is the renormalized energy spectrum. In free Fermi gases, $Z_F = 1$. As the many-body interaction increases, Z_F decreases, which leads to the upper branch appearing at significantly lower energy with respect to the RPA results. In the superfluid state, Z_F will also suppress the pairing gap, leading to a smaller pairing gap appearing in QMC simulation than the RPA results. In this paper, we do not discuss the effect of Z_F .

The band width of the single-particle excitations W is enlarged when increasing the hopping term, $W = 8t$. Moreover, along the route from $[0, 0]$ to $[\pi, \pi]$, $S(\mathbf{q}, \omega)$ has a clearly upper boundary marked by the red arrow in panel (b), and it can be described as:

$$E_u = W \sin(\mathbf{q}/2) = 8t \sin(\mathbf{q}/2). \quad (10)$$

The other contour marked by the white arrow in panel (b) can be obtained as:

$$E_d = 1.83 \sin(\mathbf{q}) \quad (11)$$

with $t/U = 0.4$. The dispersion of E_d is shown by the red-dashed line. Physically E_d is not a collective mode, but an analogy to the lower boundary of one-dimensional case at $U = 0$, $E_d = 4t \sin(\mathbf{q})$ [69, 70]. In Heisenberg model, E_d is called the des Cloiseaux-Pearson (dCP) dispersions [70]. Owing to the effect of pairing gap, here $E_d = 1.83 \sin(\mathbf{q})$. The E_d as a function of \mathbf{q} is characterized by a double periodicity compared with the upper boundary case E_u . Both E_u and E_d are determined by the single-particle excitations. The single-particle excitations can be understood by using the equation: $\hbar\omega_{\mathbf{k}\mathbf{q}} = \xi_{\mathbf{k}+\mathbf{q}} - \xi_{\mathbf{k}}$. Along with $[0, 0] \rightarrow [\pi, \pi]$, $\hbar\omega_{\mathbf{k}\mathbf{q}} = 8t \sin(\mathbf{k} + \mathbf{q}/2) \sin(\mathbf{q}/2)$. When $\sin(\mathbf{k} + \mathbf{q}/2) = 1$, the maximum excitation $\hbar\omega_{\mathbf{k}\mathbf{q}}^{max} = 8t \sin(\mathbf{q}/2) = E_u$. At $n = 1$, the Fermi momentum $k_F = \pi/2$. When $\mathbf{k} = k_F$, $\hbar\omega_{\mathbf{k}\mathbf{q}} = 4t \sin(\mathbf{q}) = E_d$.

V. RESULTS AWAY FROM HALF FILLING

Doping will influence particle density and change the Fermi energy, then greatly influence dynamical excitations. The particle density $n = 1 - \delta$, where δ is the doping concentration. Here we discuss the energy and momentum dependencies of $S(\mathbf{q}, \omega)$ when the system is away from the half-filling ($n = 0.8$), and choose the particle density $n = 0.8$. In Fig. 3, we give contour plot of $S(\mathbf{q}, \omega)$ along the high symmetry directions in the BZ for different hopping strength. There are mainly three differences by comparing $n = 0.8$ with the half-filling case,

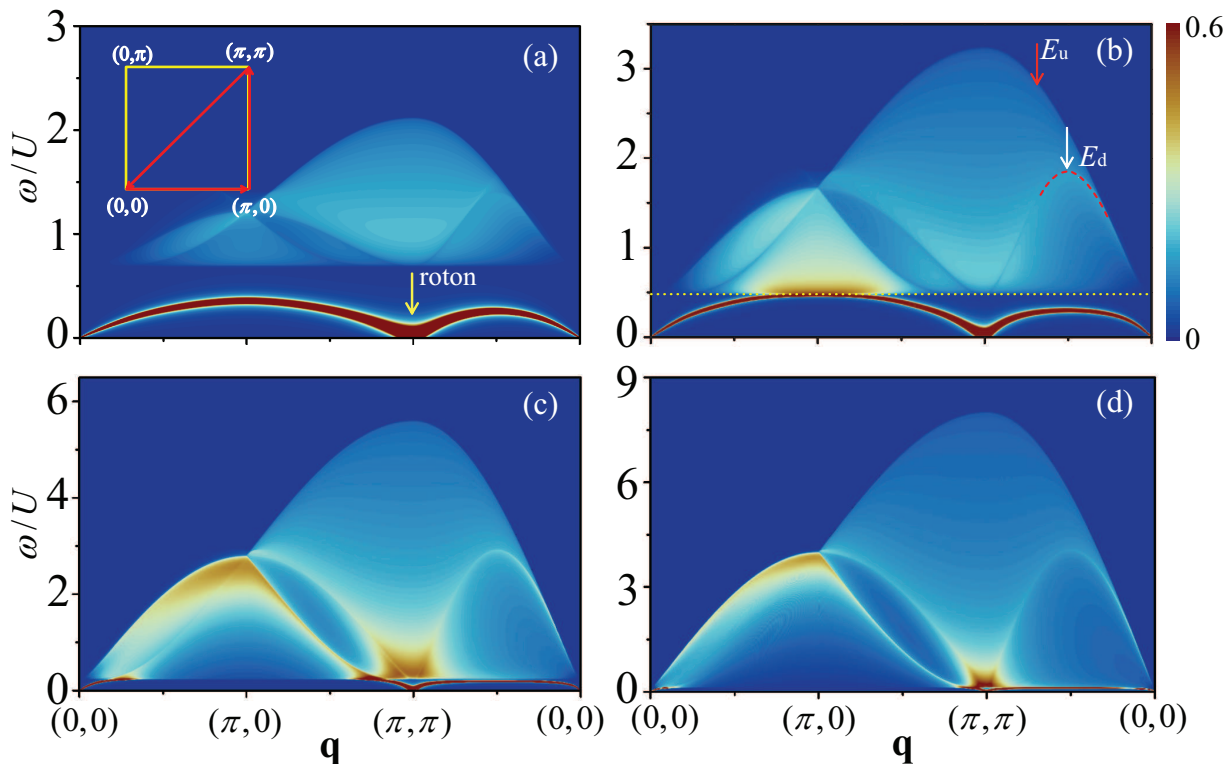


Figure 2. The color maps of the dynamical structure factor $S(\mathbf{q}, \omega)$ as functions of transferred energy and momentum along the high-symmetry directions for hopping (a) $t/U = 0.25$, (b) $t/U = 0.4$, (c) $t/U = 0.7$, and (d) $t/U = 1.0$ at half-filling $n = 1$. The red dashed line marks the dispersion of E_d . The yellow dotted line indicates the minimum energy to break a Cooper pair. Inset in (a): a quarter of the first Brillouin zone and three high symmetry directions (red arrows).

namely, the molecular excitations at $\mathbf{q} = [\pi, \pi]$, the split of E_d , and sound speed. In the following three subsections, we will introduce these differences respectively.

A. Molecular excitations at $\mathbf{q} = [\pi, \pi]$ and its related pairing gap

Compared with Fig. 2, it can be clearly seen that the minimum of the roton mode at $[\pi, \pi]$ moves upward relative to the zero energy at $n = 0.8$. So this roton mode is gapped which arises from the strong local density correlations [68]. In an optical lattice system, this roton mode is always well separated from single-particle excitations. This gapped roton mode is called the molecular Cooper-pair excitations here [71]. We show that the dynamical structure factor at $\mathbf{q} = [\pi, \pi]$ can characterize the bosonic molecular excitations (Cooper pairs excitations). To show clearly this physics, the hopping dependence of $S(\mathbf{q}, \omega)$ had been calculated, and the results of $S(\mathbf{q}, \omega)$ as a function of the transfer energy ω for different hopping strength are shown in Fig. 4. The inset figures highlight the comparison near the strength of atomic excitations in a larger energy region. Obviously $S(\mathbf{q}, \omega)$ consists of a sharp peak in the low-energy

region and a broad single-particle excitation band in the higher energy region. This sharp peak corresponds to the excitation of the bosonic molecules from a molecular condensate, while the broad single-particle excitation band is the result of atomic (particle-hole) excitations. As the hopping strength t increases (atomic interaction strength decreases), the weight of the molecular peak decreases, but the atomic excitation band increases quickly. The variation of the atomic excitation band is shown in the inset figures.

The weight of the molecular peak can be quantified by the area it covers. In Fig. 5, We display relation between the area of the molecular peak A_{peak} (pink dotted line) and the hopping t , compared with the square of the pairing gap Δ^2 (green solid line). Our results show that A_{peak} has the almost same hopping strength dependence as that of Δ^2 . Both of them are particularly large in a small t , and then decrease gradually with t from the intermediate coupling to the weak coupling regime. Therefore, our results indicate that the Δ^2 is responsible for molecular peak at $\mathbf{q} = [\pi, \pi]$. In other words, experimentally we can measure the pairing gap by detecting the dynamical structure factor at $\mathbf{q} = [\pi, \pi]$ in the BZ. It is worth noticing that this method to measure pairing gap is universal, and is also suitable for Fermi atoms with

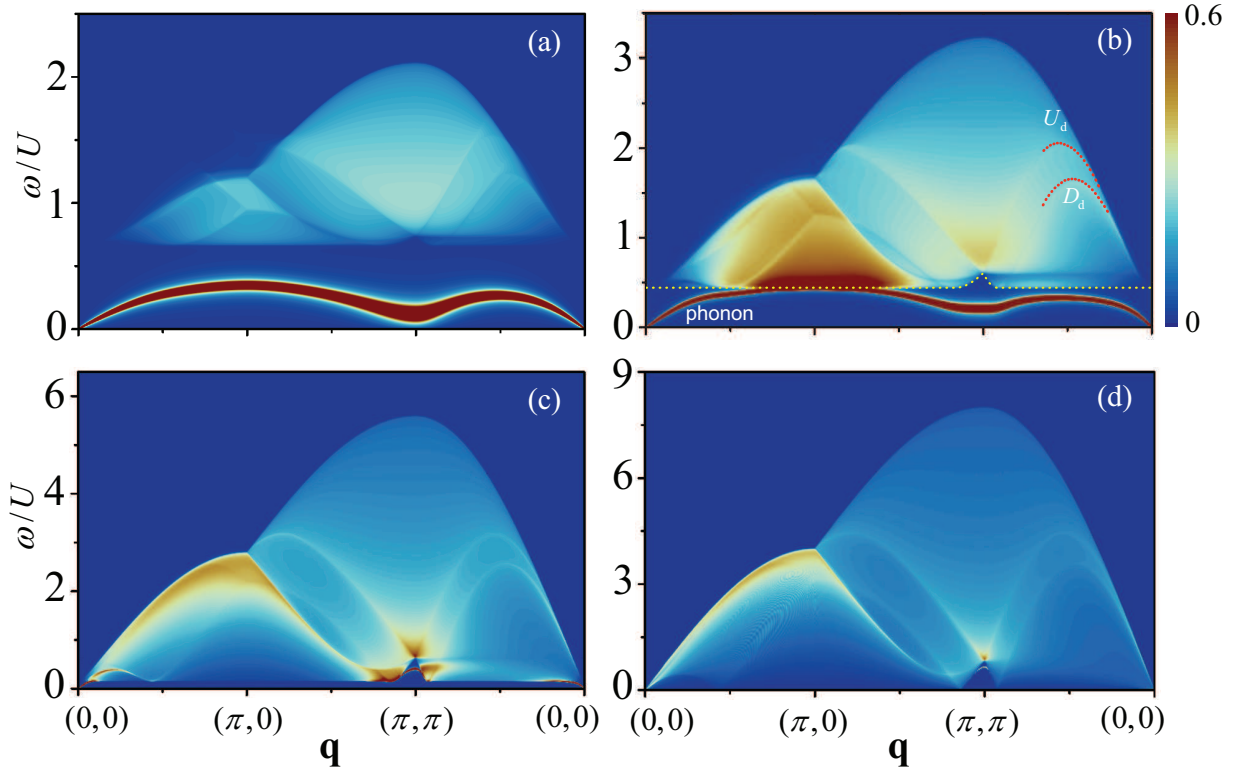


Figure 3. The color maps of $S(\mathbf{q}, \omega)$ along the high-symmetry directions for hopping strength (a) $t/U = 0.25$, (b) $t/U = 0.4$, (c) $t/U = 0.7$, and (d) $t/U = 1.0$ at $n = 0.8$. In (b), the dispersions of U_d and D_d (blue dotted lines) are the result of E_d splitting by doping.

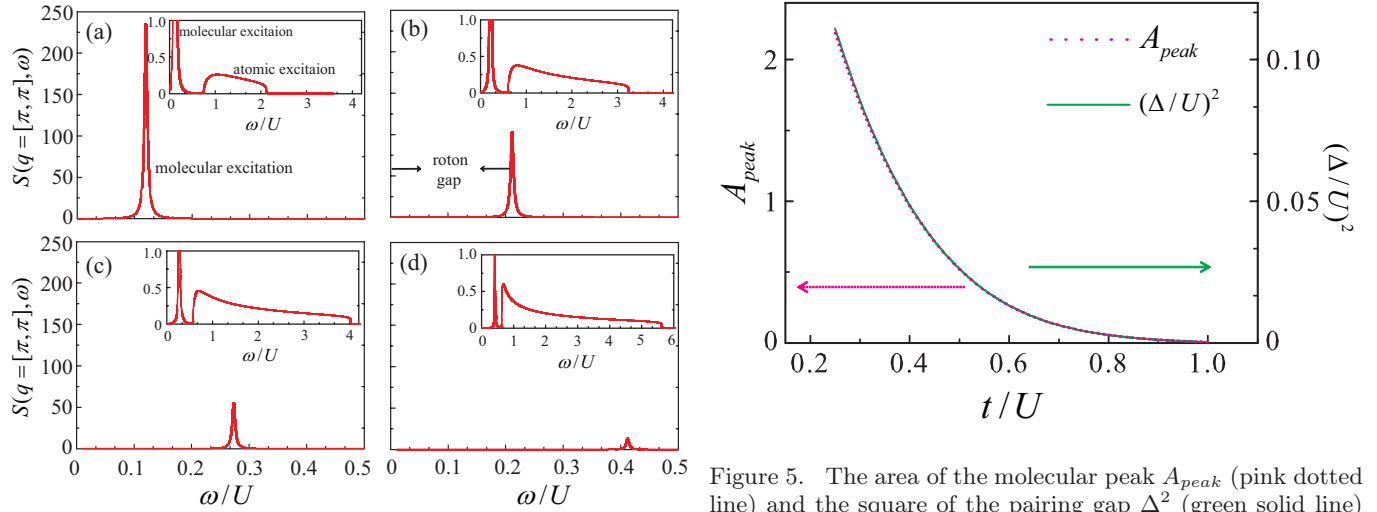


Figure 4. $S(\mathbf{q} = [\pi, \pi], \omega)$ as a function of ω for the hopping strength (a) $t/U = 0.25$, (b) $t/U = 0.4$, (c) $t/U = 0.5$, and (d) $t/U = 0.7$ at $n = 0.8$. The inset figures highlight the comparison near the strength of atomic excitations in a large energy region.

spin-orbit coupling (SOC) in an optical lattice, where the pairing gap is hard to obtain owing to the complex band structure [65].

Figure 5. The area of the molecular peak A_{peak} (pink dotted line) and the square of the pairing gap Δ^2 (green solid line) as a function of t at $n = 0.8$.

B. The split of E_d

Doping also influence the atomic excitations. Compared with the half-filling case in Fig. 2, the boundary E_d has been split owing to doping. To show this clearly, we have calculated the energy dependence of $S(\mathbf{q}, \omega)$ at $\mathbf{q} = [\pi/2, \pi/2]$. Related results of $S(\mathbf{q}, \omega)$ as a function of

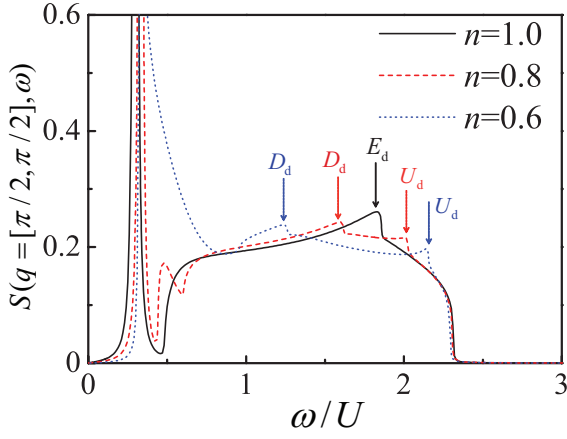


Figure 6. $S(\mathbf{q} = [\pi/2, \pi/2], \omega)$ as functions of ω for $n = 1.0$ (black solid line), $n = 0.8$ (red dashed line), and $n = 0.6$ (blue dotted line) at the hopping $t/U = 0.4$.

ω for different doping at the hopping strength $t/U = 0.4$ are plotted in Fig. 6.

At the low-energy region, a sharp excitation peak appears, and it is the signal of collective mode. Another broad band at larger energy corresponds to the atomic excitations. At half-filling (red solid line) $n = 1.0$, a characteristic peak at $\omega/U = 1.83$ (marked by the black arrow) appears and corresponds to the E_d . However, when $n = 0.8(0.6)$, it is seen clearly that E_d is split into two branches: U_d and D_d (marked by two red (blue) dotted line), which is also found in the normal state. So the split of E_d is unrelated to the interaction part $H_{\text{int}} = -\sum_{\mathbf{k}}(\Delta^* C_{\mathbf{k}\downarrow} C_{-\mathbf{k}\uparrow} + H.c.)$ in Eq. 1. Moreover, as the doping increases, the gap between U_d and D_d increases. Along $[0, 0] \rightarrow [\pi, \pi]$, the Fermi momentum $k_F = \pi/2$ at $n = 1$. As n decreases, the Fermi momentum decreases, which leads to the change of the single-particle excitations.

C. Hopping dependence of sound speed

The slope of the Goldstone mode at $\omega \rightarrow 0$ and $\mathbf{q} \rightarrow 0$ is the sound speed c_s , $c_s = \omega/|\mathbf{q}|$. The sound speed depends on the interaction strength which can be parameterized by t/U . The sound speed c_s as a function of t is plotted in Fig. 7. Our theoretical results show that the sound speed decreases with decreasing hopping strength from the intermediate coupling to the weak coupling regime, which is qualitatively consistent with the experimental results of Fermi gases ^6Li [13, 28]. The qualitatively behavior of the sound speed can be explained by a squared Fermi velocity, which will be introduced in Fig. 9.

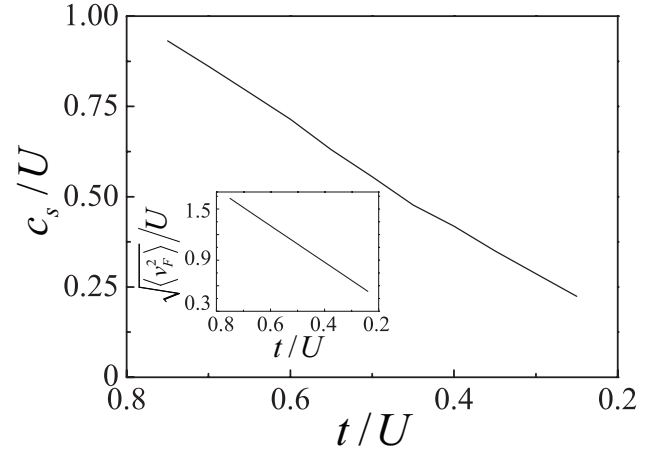


Figure 7. Sound speed c_s as a function of t at $n = 0.8$. Inset: $\sqrt{\langle v_F^2 \rangle}$ as a function of t .

VI. DOPING DEPENDENCE OF THE DYNAMICAL STRUCTURE FACTOR

Here we discuss the relation between dynamical excitations and the doping concentration. In Fig. 8, we plot $S(\mathbf{q}, \omega)$ along with the high-symmetry directions of the BZ for (a) $n = 0.6$, and (b) $n = 0.4$ with $t/U = 0.4$. Our results show that the molecular peak at $\mathbf{q} = [\pi, \pi]$

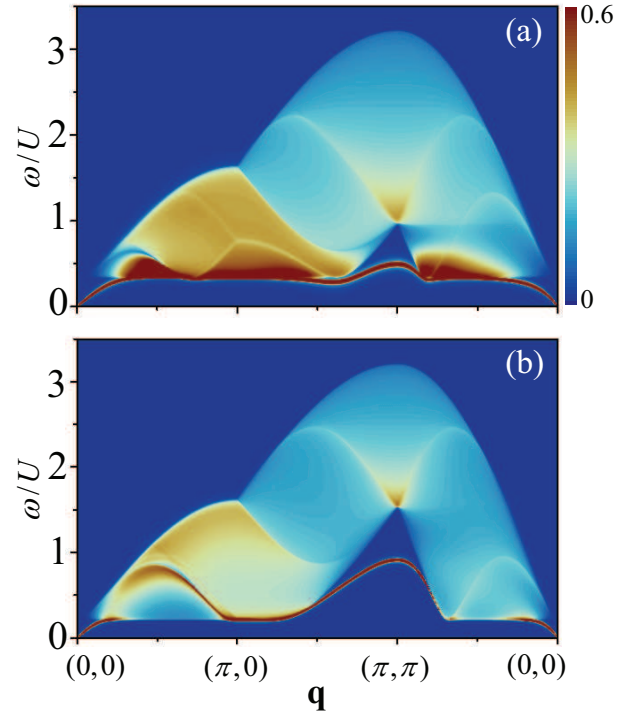


Figure 8. The color maps of $S(\mathbf{q}, \omega)$ for (a) $n = 0.6$, and (b) $n = 0.4$ with $t/U = 0.4$.

moves to the larger energy, leading to the appearance of a large roton gap. In particular, the sound speed is dop-

ing dependent. To show this issue clearly, we plot c_s as a function of n in Fig. 9a. Our results show that the sound

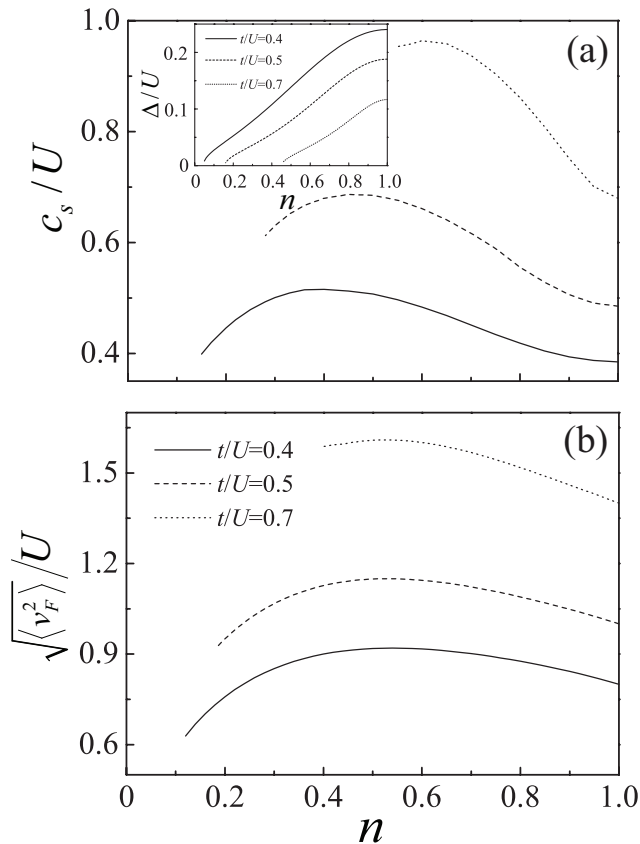


Figure 9. (a) Sound speed c_s and (b) $\sqrt{\langle v_F^2 \rangle}$ as a function of n for $t/U = 0.4$ (solid line), $t/U = 0.5$ (dashed line), and $t/U = 0.7$ (dotted line). Inset in panel (a): the corresponding pairing gap as a function of n .

speed increases initially and then decreases as n increases. This can be understood qualitatively by a weak interaction theory [73]. The sound speed is closely related to the squared Fermi velocity, $c_s = \sqrt{\langle v_F^2 \rangle} [1 - UN(0)]/2$. $N(0)$ is the density of states at the Fermi energy and is obtained by $N(0) = (2\pi)^{-2} \int d^2\mathbf{k} \delta(\xi_{\mathbf{k}})$. Therefore, $N(0)$ is proportional to the length of the Fermi surface or n . The Fermi velocity $v_F = \partial \xi_{\mathbf{k}} / \partial \mathbf{k}|_{\mathbf{k}=[k_{Fx}, k_{Fy}]}$ at a Fermi wave vector which is determined by $\xi_{\mathbf{k}=[k_{Fx}, k_{Fy}]} = 0$ together with self-consistent equations Eq. 4. So k_F , μ and Δ can be obtained self-consistently at a given n . We define $\langle v_F^2 \rangle = \frac{1}{N_0} \sum_{\mathbf{k}_F} v_F^2$, where $N_0 = 120$ is the number of points selected along the Fermi surface. We plot $\sqrt{\langle v_F^2 \rangle}$ as a function of n in Fig. 9b. It is shown that $\sqrt{\langle v_F^2 \rangle}$ has qualitatively the same n dependence as that of c_s . At half-filling, v_F is anisotropic in the BZ. When n is very small, the Fermi surface shrinks, the anisotropy of v_F decreases, the physical properties of an optical lattice can be understood using continuum Fermi gases. In the low-momentum region, the cosine function can be expanded as: $\cos k = 1 - k^2/2$, so the energy

spectrum of the optical lattice can be approximated as: $\xi_{\mathbf{k}} = Zt(k_x^2 + k_y^2) - tZ - \mu$, which has the same form with the continuum case $\xi_{\mathbf{k}} = (k_x^2 + k_y^2)/2m - \mu$. Moreover, when $n \rightarrow 0$, $N(0) \rightarrow 0$, so $c_s = \sqrt{\langle v_F^2 \rangle}/2$ which is consistent with ideal continuum Fermi gases.

VII. SUMMARY

In conclusion, the doping and hopping dependencies of the dynamical structure factor in 2D attractive Fermi-Hubbard model were studied based on RPA theory. Two collective modes were found: the phonon mode at a small transfer momentum and the roton mode at transfer momentum $\mathbf{q} = [\pi, \pi]$ regime. The roton mode is related to the Cooper pair molecular excitation. First, the area of the molecular excitation peak at $\mathbf{q} = [\pi, \pi]$ scales with the square of the pairing gap under a certain doping, which potentially indicates a new strategy to measure the pairing gap qualitatively. Second, a characteristic peak in the atomic excitation band is split into two branches when the system is away from half-filling, and the gap between them increase for a large doping. Third, the sound speed at given doping is suppressed by interaction strength.

VIII. ACKNOWLEDGEMENTS

This work was supported by the funds from the National Natural Science Foundation of China under Grant No.11547034 (H.Z.), Grants No. U23A2073 (P.Z.)

Perceptually uniform color maps ('roma') are used in this study (Crameri 2018)

IX. APPENDIX

The mean-field response function χ^0 of 2D interacting Fermi atoms in a square optical lattice is numerically calculated, and all 6 independent matrices elements of χ^0 are

$$\chi_{11}^0 = \frac{1}{4} \sum_{\mathbf{k}} \left[1 + \frac{\xi_{\mathbf{k}} \xi_{\mathbf{k}+\mathbf{q}}}{E_{\mathbf{k}} E_{\mathbf{k}+\mathbf{q}}} \right] F_{\mathbf{k},\mathbf{q}}^{(1)} + \frac{1}{4} \sum_{\mathbf{k}} \left[1 - \frac{\xi_{\mathbf{k}} \xi_{\mathbf{k}+\mathbf{q}}}{E_{\mathbf{k}} E_{\mathbf{k}+\mathbf{q}}} \right] F_{\mathbf{k},\mathbf{q}}^{(2)},$$

$$\chi_{12}^0 = -\frac{1}{4} \sum_{\mathbf{k}} \frac{\Delta^2}{E_{\mathbf{k}} E_{\mathbf{k}+\mathbf{q}}} \left[F_{\mathbf{k},\mathbf{q}}^{(1)} - F_{\mathbf{k},\mathbf{q}}^{(2)} \right],$$

$$\begin{aligned}\chi_{13}^0 &= -\frac{\Delta}{4} \sum_{\mathbf{k}} \frac{\xi_{\mathbf{k}} + \xi_{\mathbf{k}+\mathbf{q}}}{2E_{\mathbf{k}}E_{\mathbf{k}+\mathbf{q}}} \left[F_{\mathbf{k},\mathbf{q}}^{(1)} - F_{\mathbf{k},\mathbf{q}}^{(2)} \right] \\ &+ \frac{\Delta}{4} \sum_{\mathbf{k}} \frac{E_{\mathbf{k}+\mathbf{q}} - E_{\mathbf{k}}}{2E_{\mathbf{k}}E_{\mathbf{k}+\mathbf{q}}} F_{\mathbf{k},\mathbf{q}}^{(3)} \\ &- \frac{\Delta}{4} \sum_{\mathbf{k}} \frac{E_{\mathbf{k}+\mathbf{q}} + E_{\mathbf{k}}}{2E_{\mathbf{k}}E_{\mathbf{k}+\mathbf{q}}} F_{\mathbf{k},\mathbf{q}}^{(4)},\end{aligned}$$

$$\begin{aligned}\chi_{14}^0 &= -\frac{\Delta}{4} \sum_{\mathbf{k}} \frac{\xi_{\mathbf{k}} + \xi_{\mathbf{k}+\mathbf{q}}}{2E_{\mathbf{k}}E_{\mathbf{k}+\mathbf{q}}} \left[F_{\mathbf{k},\mathbf{q}}^{(1)} - F_{\mathbf{k},\mathbf{q}}^{(2)} \right] \\ &- \frac{\Delta}{4} \sum_{\mathbf{k}} \frac{E_{\mathbf{k}+\mathbf{q}} - E_{\mathbf{k}}}{2E_{\mathbf{k}}E_{\mathbf{k}+\mathbf{q}}} F_{\mathbf{k},\mathbf{q}}^{(3)} \\ &+ \frac{\Delta}{4} \sum_{\mathbf{k}} \frac{E_{\mathbf{k}+\mathbf{q}} + E_{\mathbf{k}}}{2E_{\mathbf{k}}E_{\mathbf{k}+\mathbf{q}}} F_{\mathbf{k},\mathbf{q}}^{(4)},\end{aligned}$$

$$\begin{aligned}\chi_{43}^0 &= \frac{1}{4} \sum_{\mathbf{k}} \left[1 - \frac{\xi_{\mathbf{k}}\xi_{\mathbf{k}+\mathbf{q}}}{E_{\mathbf{k}}E_{\mathbf{k}+\mathbf{q}}} \right] F_{\mathbf{k},\mathbf{q}}^{(1)} \\ &+ \frac{1}{4} \sum_{\mathbf{k}} \left[1 + \frac{\xi_{\mathbf{k}}\xi_{\mathbf{k}+\mathbf{q}}}{E_{\mathbf{k}}E_{\mathbf{k}+\mathbf{q}}} \right] F_{\mathbf{k},\mathbf{q}}^{(2)} \\ &+ \frac{1}{4} \sum_{\mathbf{k}} \left[\frac{\xi_{\mathbf{k}}}{E_{\mathbf{k}}} - \frac{\xi_{\mathbf{k}+\mathbf{q}}}{E_{\mathbf{k}+\mathbf{q}}} \right] F_{\mathbf{k},\mathbf{q}}^{(3)} \\ &- \frac{1}{4} \sum_{\mathbf{k}} \left[\frac{\xi_{\mathbf{k}}}{E_{\mathbf{k}}} + \frac{\xi_{\mathbf{k}+\mathbf{q}}}{E_{\mathbf{k}+\mathbf{q}}} \right] F_{\mathbf{k},\mathbf{q}}^{(4)},\end{aligned}$$

$$\begin{aligned}\chi_{34}^0 &= \frac{1}{4} \sum_{\mathbf{k}} \left[1 - \frac{\xi_{\mathbf{k}}\xi_{\mathbf{k}+\mathbf{q}}}{E_{\mathbf{k}}E_{\mathbf{k}+\mathbf{q}}} \right] F_{\mathbf{k},\mathbf{q}}^{(1)} \\ &+ \frac{1}{4} \sum_{\mathbf{k}} \left[1 + \frac{\xi_{\mathbf{k}}\xi_{\mathbf{k}+\mathbf{q}}}{E_{\mathbf{k}}E_{\mathbf{k}+\mathbf{q}}} \right] F_{\mathbf{k},\mathbf{q}}^{(2)} \\ &- \frac{1}{4} \sum_{\mathbf{k}} \left[\frac{\xi_{\mathbf{k}}}{E_{\mathbf{k}}} - \frac{\xi_{\mathbf{k}+\mathbf{q}}}{E_{\mathbf{k}+\mathbf{q}}} \right] F_{\mathbf{k},\mathbf{q}}^{(3)} \\ &+ \frac{1}{4} \sum_{\mathbf{k}} \left[\frac{\xi_{\mathbf{k}}}{E_{\mathbf{k}}} + \frac{\xi_{\mathbf{k}+\mathbf{q}}}{E_{\mathbf{k}+\mathbf{q}}} \right] F_{\mathbf{k},\mathbf{q}}^{(4)}.\end{aligned}$$

The corresponding functions in above equations $F_{\mathbf{k},\mathbf{q}}^{(1)}$, $F_{\mathbf{k},\mathbf{q}}^{(2)}$, $F_{\mathbf{k},\mathbf{q}}^{(3)}$, $F_{\mathbf{k},\mathbf{q}}^{(4)}$ are defined as

$$\begin{aligned}F_{\mathbf{k},\mathbf{q}}^{(1)} &= A(\mathbf{k}, \mathbf{q}, i\omega_n) - B(\mathbf{k}, \mathbf{q}, i\omega_n), \\ F_{\mathbf{k},\mathbf{q}}^{(2)} &= C(\mathbf{k}, \mathbf{q}, i\omega_n) - D(\mathbf{k}, \mathbf{q}, i\omega_n), \\ F_{\mathbf{k},\mathbf{q}}^{(3)} &= A(\mathbf{k}, \mathbf{q}, i\omega_n) + B(\mathbf{k}, \mathbf{q}, i\omega_n), \\ F_{\mathbf{k},\mathbf{q}}^{(4)} &= C(\mathbf{k}, \mathbf{q}, i\omega_n) + D(\mathbf{k}, \mathbf{q}, i\omega_n),\end{aligned}\quad (12)$$

where

$$\begin{aligned}A(\mathbf{k}, \mathbf{q}, i\omega_n) &= \frac{f(E_{\mathbf{k}}) - f(E_{\mathbf{k}+\mathbf{q}})}{i\omega_n + (E_{\mathbf{k}} - E_{\mathbf{k}+\mathbf{q}})} \\ B(\mathbf{k}, \mathbf{q}, i\omega_n) &= \frac{f(E_{\mathbf{k}}) - f(E_{\mathbf{k}+\mathbf{q}})}{i\omega_n - (E_{\mathbf{k}} - E_{\mathbf{k}+\mathbf{q}})} \\ C(\mathbf{k}, \mathbf{q}, i\omega_n) &= \frac{1 - f(E_{\mathbf{k}}) - f(E_{\mathbf{k}+\mathbf{q}})}{i\omega_n - (E_{\mathbf{k}} + E_{\mathbf{k}+\mathbf{q}})} \\ D(\mathbf{k}, \mathbf{q}, i\omega_n) &= \frac{1 - f(E_{\mathbf{k}}) - f(E_{\mathbf{k}+\mathbf{q}})}{i\omega_n + (E_{\mathbf{k}} + E_{\mathbf{k}+\mathbf{q}})},\end{aligned}\quad (13)$$

$f(E_{\mathbf{k}})$ and $f(E_{\mathbf{k}+\mathbf{q}})$ are Fermi distributions.

-
- [1] M. Feld, B. Fröhlich, E. Vogt, M. Koschorreck and M. Köhl, *Observation of a pairing pseudogap in a two-dimensional Fermi gas*, *Nature* **480**, 75 (2011).
- [2] J. T. Stewart, J. P. Gaebler and D. S. Jin, *Using photoemission spectroscopy to probe a strongly interacting Fermi gas*, *Nature* **454**, 744 (2008).
- [3] B. Fröhlich, M. Feld, E. Vogt, M. Koschorreck, W. Zwerger and M. Köhl, *Radio-Frequency Spectroscopy of a Strongly Interacting Two-Dimensional Fermi Gas*, *Phys. Rev. Lett.* **106**, 105301 (2011).
- [4] C. Chin, M. Bartenstein, A. Altmeyer, S. Riedl, S. Jochim, J. Hecker Denschlag, and R. Grimm, *Observation of the Pairing Gap in a Strongly Interacting Fermi Gas*, *Science* **305**, 1128 (2004).
- [5] A. T. Sommer, L. W. Cheuk, M. J. H. Ku, W. S. Bakr, and M. W. Zwierlein, *Evolution of Fermion Pairing from Three to Two Dimensions*, *Phys. Rev. Lett.* **108**, 045302 (2012).
- [6] H. Zhai, *Degenerate quantum gases with spin-orbit coupling: a review*, *Rep. Prog. Phys.* **78**, 026001 (2015).
- [7] L. W. Cheuk, A. T. Sommer, Z. Hadzibabic, T. Yefsah, W. S. Bakr and M. W. Zwierlein, *Spin-Injection on Spectroscopy of a Spin-Orbit Coupled Fermi gas*, *Phys. Rev. Lett.* **109**, 095302 (2012).
- [8] P. Wang, Z.-Q. Yu, Z. Fu, J. Miao, L. Huang, S. Chai, H. Zhai and J. Zhang, *Spin-Orbit Coupled Degenerate Fermi Gases*, *Phys. Rev. Lett.* **109**, 095301 (2012).
- [9] Z.-Y. Wang, X.-C. Cheng, B.-Z. Wang, J.-Y. Zhang, Y.-H. Lu, C.-R. Yi, S. Niu, Y. Deng, X.-J. Liu, S. Chen, and J.-W. Pan, *Realization of an ideal Weyl semimetal band in a quantum gas with 3D Spin-Orbit coupling*, *Science* **372**, 271 (2021).
- [10] F. Wu, G.-C. Guo, W. Zhang, and W. Yi, *Unconventional Superfluid in a Two-Dimensional Fermi gas with Anisotropic Spin-Orbit Coupling and Zeeman fields*, *Phys. Rev. Lett.* **110**, 110401 (2013).
- [11] R. Han, F. Yuan and H. Zhao, *Phase diagram, band structure and density of states in two-dimensional attractive Fermi-Hubbard model with Rashba spin-orbit coupling*, *New J. Phys.* **25**, 023011 (2023).

- [12] G. Veeravalli, E. Kuhnle, P. Dyke, and C. J. Vale, *Bragg Spectroscopy of a Strongly Interacting Fermi Gas*, *Phys. Rev. Lett.* **101**, 250403 (2008).
- [13] S. Hoinka, P. Dyke, M. G. Lingham, J. J. Kinnunen, G. M. Bruun and C. J. Vale, *Goldstone mode and pair-breaking excitations in atomic Fermi superfluid*, *Nat. Phys.* **13**, 943 (2017).
- [14] H. Biss, L. Sobirey, N. Luick, M. Bohlen, J. J. Kinnunen, G. M. Bruun, T. Lompe, and H. Moritz, *Excitation Spectrum and Superfluid Gap of an Ultracold Fermi Gas*, *Phys. Rev. Lett.* **128**, 100401 (2022).
- [15] R. Senaratne, D. Cavazos-Cavazos, S. Wang, F. He, Y.-T. Chang, A. Kafle, H. Pu, X.-W. Guan, and R. G. Hulet, *Spin-charge separation in a 1D Fermi gas with tunable interactions*, *Science* **376**, 1305 (2022).
- [16] X. Li, X. Luo, S. Wang, K. Xie, X. P. Liu, H. Hu, Y.-A. Chen, X.-C. Yao and J. W. Pan, *Second sound attenuation near quantum criticality*, *Science*, **375**, 528 (2022).
- [17] G. Pagano, M. Mancini, G. Cappellini, P. Lombardi, F. Schöfer, H. Hu, X.-J. Liu, J. Catani, C. Sias, M. Inguscio and L. Fallani, *A one-dimensional liquid of fermions with tunable spin*, *Nat. Phys.* **10**, 198 (2014).
- [18] P. Dyke, S. Musolino, H. Kurkjian, D. J. M. Ahmed-Braun, A. Pennings, I. Herrera, S. Hoinka, S. J. J. M. F. Kokkelmans, V. E. Colussi, C. J. Vale, *Higgs oscillations in a unitary Fermi superfluid*, [arXiv:2310.03452](https://arxiv.org/abs/2310.03452).
- [19] R. Combescot, S. Giorgini and S. Stringari, *Molecular signatures in the structure factor of an interacting Fermi gas*, *Europhys. Lett.* **75**, 695 (2006).
- [20] R. Combescot, M. Yu. Kagan, and S. Stringari, *Collective mode of homogeneous superfluid Fermi gases in the BEC-BCS crossover*, *Phys. Rev. A* **74**, 042717 (2006).
- [21] P. Zou, E. D. Kuhnle, C. J. Vale, and H. Hu, *Quantitative comparison between theoretical predictions and experimental results for Bragg spectroscopy of a strongly interacting Fermi superfluid*, *Phys. Rev. A* **82**, 061605(R) (2010).
- [22] P. Zou, F. Dalfovo, R. Sharma, X. J. Liu and H. Hu, *Dynamic structure factor of a strongly correlated Fermi superfluid within a density functional theory approach*, *New J. Phys.* **18**, 113044 (2016).
- [23] P. Zou, H. Hu, and X.-J. Liu, *Low-momentum dynamic structure factor of a strongly interacting Fermi gas at finite temperature: The Goldstone phonon and its Landau damping*, *Phys. Rev. A* **98**, 011602(R) (2018).
- [24] H. Hu, P. Zou, and X.-J. Liu, *Low-momentum dynamic structure factor of a strongly interacting Fermi gas at finite temperature: A two-fluid hydrodynamic description*, *Phys. Rev. A* **97**, 023615 (2018).
- [25] P. Zou, H. Zhao, L. He, X.-J. Liu, and H. Hu, *Dynamic structure factors of a strongly interacting Fermi superfluid near an orbital Feshbach resonance across the phase transition from BCS to Sarma superfluid*, *Phys. Rev. A* **103**, 053310 (2021).
- [26] E. D. Kuhnle, H. Hu, X.-J. Liu, P. Dyke, M. Mark, P. D. Drummond, P. Hannaford, and C. J. Vale, *Universal Behavior of Pair Correlations in a Strongly Interacting Fermi Gas*, *Phys. Rev. Lett.* **105**, 070402 (2010).
- [27] S. Watabe, and T. Nikuni, *Dynamic structure factor of the normal Fermi gas from the collisionless to the hydrodynamic regime*, *Phys. Rev. A* **82**, 033622 (2010).
- [28] L. Sobirey, H. Biss, N. Luick, M. Bohlen, H. Moritz, and T. Lompe, *Observing the Influence of Reduced Dimensionality on Fermionic Superfluids*, *Phys. Rev. Lett.* **129**, 083601 (2022).
- [29] E. Vitali, H. Shi, M. Qin, and S. Zhang, *Visualizing the BEC-BCS crossover in a two-dimensional Fermi gas: Pairing gaps and dynamical response functions from ab initio computations*, *Phys. Rev. A* **96**, 061601(R) (2017).
- [30] H. Zhao, X. Gao, W. Liang, P. Zou and F. Yuan, *Dynamical structure factors of a two-dimensional Fermi superfluid within random phase approximation*, *New J. Phys.* **22**, 093012 (2020).
- [31] Z. Gao, L. He, H. Zhao, S.-G. Peng, and P. Zou, *Dynamic structure factor of one-dimensional Fermi superfluid with spin-orbit coupling*, *Phys. Rev. A* **107**, 013304 (2023).
- [32] I. Bloch, J. Dalibard and W. Zwerger, *Many-body physics with ultracold gases*, *Rev. Mod. Phys.* **80**, 885 (2008).
- [33] Z. Wu, L. Zhang, W. Sun, X.-T. Xu, B.-Z. Wang, S.-C. Ji, Y. Deng, S. Chen, X.-J. Liu, and J.-W. Pan, *Realization of two-dimensional spin-orbit coupling for Bose-Einstein condensates*, *Science* **354**, 83 (2016).
- [34] M. Greiner, O. Mandel, T. Esslinger, T. W. Hänsch, and I. Bloch, *Quantum phase transition from a superfluid to a Mott insulator in a gas of ultracold atoms*, *Nature* **415**, 39 (2002).
- [35] I. B. Spielman, W. D. Phillips, and J. V. Porto, *Condensate Fraction in a 2D Bose Gas Measured across the Mott-Insulator Transition*, *Phys. Rev. Lett.* **100**, 120402 (2008).
- [36] C. K. Thomas, T. H. Barter, T.-H. Leung, M. Okano, G.-B. Jo, J. Guzman, I. Kimchi, A. Vishwanath, and D. M. Stamper-Kurn, *Mean-Field Scaling of the Superfluid to Mott Insulator Transition in a 2D Optical Superlattice*, *Phys. Rev. Lett.* **119**, 100402 (2017).
- [37] R. Jördens, N. Strohmaier, K. Günter, H. Moritz, and T. Esslinger, *A Mott insulator of fermionic atoms in an optical lattice*, *Nature* **455**, 204 (2008).
- [38] U. Schneider, L. Hackermüller, S. Will, Th. Best, I. Bloch, T. A. Costi, R. W. Helmes, D. Rasch, and A. Rosch, *Metallic and insulating phases of repulsively interacting fermions in a 3D optical lattice*, *Science* **322**, 1520 (2008).
- [39] D. Greif, T. Uehlinger, G. Jotzu, L. Tarruell, and T. Esslinger, *Short-range quantum magnetism of ultracold fermions in an optical lattice*, *Science* **340**, 1307 (2013).
- [40] R. A. Hart, P. M. Duarte, T.-L. Yang, X. Liu, T. Paiva, E. Khatami, R. T. Scalettar, N. Trivedi, D. A. Huse, and R. G. Hulet, *Observation of antiferromagnetic correlations in the Hubbard model with ultracold atoms*, *Nature* **519**, 211 (2015).
- [41] M. F. Parsons, A. Mazurenko, C. S. Chiu, G. Ji, D. Greif and M. Greiner, *Site-resolved measurement of the spin-correlation function in the Fermi-Hubbard model*, *Science* **353**, 1253 (2016).
- [42] L. W. Cheuk, M. A. Nichols, K. R. Lawrence, M. Okan, H. Zhang, E. Khatami, N. Trivedi, T. Paiva, M. Rigol, and M. W. Zwierlein, *Observation of spatial charge and spin correlations in the 2D Fermi-Hubbard model*, *Science* **353**, 1260 (2016).
- [43] J. Koepsell, D. Bourgund, P. Sompet, S. Hirthe, A. Bohrdt, Y. Wang, F. Grusdt, E. Demler, G. Salomon, C. Gross, and I. Bloch, *Microscopic evolution of doped Mott insulators from polaronic metal to Fermi liquid*, *Science* **374**, 82 (2021).

- [44] M. Boll, T. A. Hilker, G. Salomon, A. Omran, J. Nespolo, L. Pollet, I. Bloch, and C. Gross, *Spin-and density-resolved microscopy of antiferromagnetic correlations in Fermi-Hubbard chains*, *Science* **353**, 1257 (2016).
- [45] P. T. Brown, D. Mitra, E. Guardado-Sanchez, P. Schauß, S. S. Kondov, E. Khatami, T. Paiva, N. Trivedi, D. A. Huse, and W. S. Bakr, *Spin-imbalance in a 2D Fermi-Hubbard system*, *Science* **357**, 1385 (2017).
- [46] D. P. Arovas, E. Berg, S. A. Kivelson, S. Raghu, *The Hubbard Model*, *Annual Review of Condensed Matter Physics* **13**, 239 (2022).
- [47] R. T. Scalettar, E. Y. Loh, J. E. Gubernatis, A. Moreo, S. R. White, D. J. Scalapino, R. L. Sugar, and E. Dagotto, *Phase diagram of the two-dimensional negative- U Hubbard model*, *Phys. Rev. Lett.* **62**, 1407 (1989).
- [48] B. Kyung, S. Allen, and A.-M. S. Tremblay, *Pairing fluctuations and pseudogaps in the attractive Hubbard model*, *Phys. Rev. B* **64**, 075116 (2001).
- [49] C. Honerkamp, and W. Hofstetter, *Ultracold Fermions and the $SU(N)$ Hubbard Model*, *Phys. Rev. Lett.* **92**, 170403 (2004).
- [50] R. Mondaini, P. Nikolić, and M. Rigol, *Mott-insulator-to-superconductor transition in a two-dimensional superlattice*, *Phys. Rev. A* **92**, 013601 (2015).
- [51] E. Cocchi, L. A. Miller, J. H. Drewes, M. Koschorreck, D. Pertot, F. Brennecke, and M. Köhl, *Equation of state of the two-dimensional Hubbard model*, *Phys. Rev. Lett.* **116**, 175301 (2016).
- [52] N. Strohmaier, Y. Takasu, K. Günter, R. Jördens, M. Köhl, H. Moritz, and T. Esslinger, *Interaction-controlled transport of an ultracold Fermi gas*, *Phys. Rev. Lett.* **99**, 220601 (2007).
- [53] A. F. Ho, M. A. Cazalilla, and T. Giamarchi, *Quantum simulation of the Hubbard model: the attractive route*, *Phys. Rev. A* **79**, 033620 (2009).
- [54] A. Moreo, D. J. Scalapino, *Cold attractive spin polarized Fermi lattice gases and the doped positive U Hubbard model*, *Phys. Rev. Lett.* **98**, 216402 (2007).
- [55] J. Gukelberger, S. Lienert, E. Kozik, L. Pollet, and M. Troyer, *Fulde-Ferrell-Larkin-Ovchinnikov pairing as leading instability on the square lattice*, *Phys. Rev. B* **94**, 075157 (2016).
- [56] T. Paiva, R. R. dos Santos, R. T. Scalettar, and P. J. H. Denteneer, *Critical temperature for the two-dimensional attractive Hubbard model*, *Phys. Rev. B* **69**, 184501 (2004).
- [57] V. B. Shenoy, *Phase diagram of the attractive Hubbard model with inhomogeneous interactions*, *Phys. Rev. B* **78**, 134503 (2008).
- [58] D. Mitra, P. T. Brown, E. Guardado-Sanchez, S. S. Kondov, T. Devakul, D. A. Huse, P. Schauß, and W. S. Bakr, *Quantum gas microscopy of an attractive Fermi-Hubbard system*, *Nat. Phys.* **14**, 173 (2018).
- [59] P. T. Brown, E. Guardado-Sanchez, B. M. Spar, E. W. Huang, T. P. Devereaux, and W. S. Bakr, *Angle-resolved photoemission spectroscopy of a Fermi-Hubbard system*, *Nat. Phys.* **16**, 26 (2020).
- [60] L. Hackermüller, U. Schneider, M. Moreno-Cardoner, T. Kitagawa, T. Best, S. Will, E. Demler, E. Altman, I. Bloch, and B. Paredes, *Anomalous Expansion of Attractively Interacting Fermionic Atoms in an Optical Lattice*, *Science* **327**, 1621 (2010).
- [61] M. Gall, C. F. Chan, N. Wurz, and M. Köhl, *Simulating a Mott Insulator Using Attractive Interaction*, *Phys. Rev. Lett.* **124**, 010403 (2020).
- [62] U. Schneider, L. Hackermüller, J. P. Ronzheimer, S. Will, S. Braun, T. Best, I. Bloch, E. Demler, S. Mandt, D. Rasch, and A. Rosch, *Fermionic transport and out-of-equilibrium dynamics in a homogeneous Hubbard model with ultracold atoms*, *Nat. Phys.* **8**, 213 (2012).
- [63] T. Hartke, B. Oreg, C. Turnbaugh, N. Jia, M. Zwierlein, *Direct observation of nonlocal fermion pairing in an attractive Fermi-Hubbard gas*, *Science* **381**, 82 (2023).
- [64] E. Vitali, P. Kelly, A. Lopez, G. Bertaina, and D. E. Galli, *Dynamical structure factor of a fermionic super-solid on an optical lattice*, *Phys. Rev. A* **102**, 053324 (2020).
- [65] H. Zhao, R. Han, L. Qin, F. Yuan, and P. Zou, *A universal pairing gap measurement proposal by dynamical excitations in 2D doped attractive Fermi-Hubbard model with spin-orbit coupling*, [arXiv:2401.17488](https://arxiv.org/abs/2401.17488).
- [66] X.-J. Liu, H. Hu, A. Minguzzi, and M. P. Tosi, *Collective oscillations of a confined Bose gas at finite temperature in the random-phase approximation*, *Phys. Rev. A* **69**, 043605 (2004).
- [67] L. He, *Dynamic density and spin responses of a superfluid Fermi gas in the BCS-BEC crossover: Path integral formulation and pair fluctuation theory*, *Ann. Phys.* **373**, 470 (2016).
- [68] R. Ganesh, A. Paramekanti, and A. A. Burkov, *Collective modes and superflow instabilities of strongly correlated Fermi superfluids*, *Phys. Rev. A* **80**, 043612 (2009).
- [69] R. Han, F. Yuan, and H. Zhao, *Single-particle excitations and metal-insulator transition of ultracold Fermi atoms in one-dimensional optical lattice with spin-orbit coupling*, *Europhys. Lett.* **139**, 25001 (2022).
- [70] A. Nocera, N. D. Patel, J. Fernandez-Baca, E. Dagotto, and G. Alvarez, *Magnetic excitation spectra of strongly correlated quasi-one-dimensional systems: Heisenberg versus Hubbard-like behavior*, *Phys. Rev. B* **94**, 205145 (2016).
- [71] Shoucheng Zhang, *Pseudospin Symmetry and New Collective Modes of the Hubbard Model*, *Phys. Rev. Lett.* **65**, 120 (1990).
- [72] M. Qin, T. Schäfer, S. Andergassen, P. Corboz, and E. Gull, *The Hubbard Model: A Computational Perspective*, *Annual Review of Condensed Matter Physics* **13**, 275 (2022).
- [73] L. Belkhir and M. Randeria, *Crossover from Cooper pairs to composite bosons: A generalized RPA analysis of collective excitations*, *Phys. Rev. B* **49**, 6829 (1994).
- [74] T. Schäfer, N. Wentzell, F. Šimkovic, Y.-Y. He, C. Hille, M. Klett, C. J. Eckhardt, B. Arzhang, V. Harkov, F. M. Le Régent, A. Kirsch, Y. Wang, A. J. Kim, E. Kozik, E. A. Stepanov, A. Kauch, S. Andergassen, P. Hansmann, D. Rohe, Y. M. Vilch, J. P. F. LeBlanc, S. Zhang, A.-M. S. Tremblay, M. Ferrero, O. Parcollet, and A. Georges, *Tracking the Footprints of Spin Fluctuations: A Multi-Method, MultiMessenger Study of the Two-Dimensional Hubbard Model*, *Phys. Rev. X* **11**, 011058 (2021).
- [75] H. Hafermann, E. G. C. P. van Loon, M. I. Katsnelson, A. I. Lichtenstein, and O. Parcollet, *Collective charge excitations of strongly correlated electrons, vertex corrections, and gauge invariance*, *Phys. Rev. B* **90**, 235105 (2014).
- [76] S. Feng, L. Kuang, and H. Zhao, *Electronic structure of cuprate superconductors in a full charge-spin recombination scheme*, *Physica C* **517**, 5 (2015).

- [77] P. W. Anderson, P. A. Lee, M. Randeria, T. M. Rice, N. Trivedi and F. C. Zhang, *The physics behind high-temperature superconducting cuprates: the 'plain vanilla' version of RVB*, *J. Phys.: Condens. Matter* **16**, R755 (2004).